


# Interaction of multiply charged ions with large free silver nanoparticles: Multielectron capture, fragmentation, and sputtering phenomena

Arkadiusz P. Mika, Patrick Rousseau <sup>\*</sup>, Alicja Domaracka, and Bernd A. Huber  
Normandie Université, ENSICAEN, UNICAEN, CEA, CNRS, CIMAP, 14000 Caen, France

 (Received 2 May 2019; revised manuscript received 19 July 2019; published 30 August 2019)

We report on the interaction of multiply charged ions at keV energies with free Ag nanoparticles with diameters of  $\sim 6$  nm (containing about 6600 Ag atoms). As the ionization energy increases only very slowly with the degree of ionization, multielectron capture processes are very likely to occur in peripheral collisions with large cluster sizes. However, due to the large particle size, the produced highly charged Ag nanoparticles are mostly stable. For projectile charge states below  $q = 8$  the geometrical cross section overcomes the cross section for peripheral electron transfer, and penetrating collisions become dominant. Therefore, these collisions can be described as ion collision with a nanosurface, where the distribution of small-size fragments with  $n < 20$  is due to sputtering events from the nanoparticle surface. This is in contrast to nanoparticles with a smaller diameter ( $< 2$  nm), where small fragments are produced by fission of multiply charged clusters.

DOI: [10.1103/PhysRevB.100.075439](https://doi.org/10.1103/PhysRevB.100.075439)

## I. INTRODUCTION

Ion collisions with nanoparticles (NPs) play an important role for the sputtering of surfaces [1], aerosols [2], and dust particles in space [3]. Many experiments have been performed with NPs which were deposited on substrates. It was shown that it is possible to modify the character and structure of the NPs [4] and to determine the sputter yields as a function of the material, the NP size, and the projectile [5–7].

The first studies of the interaction of ions with free metallic clusters in the gas phase were performed in the 1990s, when sodium clusters containing typically 200 atoms were irradiated with multiply charged ions [8,9]. In these studies the stability of multiply charged sodium clusters as well as their dynamic behavior was analyzed by coincidence measurements. Compared with nanosecond-laser experiments [10–12], ion beams allowed us to extend studies to much higher charge states formed with much lower internal energies. These experiments showed that above so-called appearance sizes multiply charged clusters might be metastable and that for smaller cluster sizes they decay by fission processes, yielding singly charged small fragments.

More recently, the interest in ion collisions with larger metallic nanoparticles strongly increased due to their possible use as radiosensitizers in ion beam cancer therapy [13,14]. Thus, it has been shown that ion irradiation of cell cultures by  $C^{6+}$  ions at 256 MeV/u, with and without administering metallic nanoparticles in the nanometer size range, reduced the survival rate of the infected molecules by about 30% [15]. Also gadolinium, silver, gold, and platinum nanoparticles have been tested with similar promising results [16].

However, up to now the exact mechanisms and their relative importance still have to be clarified. It is commonly understood that the majority of the deposited energy dose is

related to ionizations and excitations produced by secondary electrons. The majority have energies below 50 eV [17], which allows them to contribute to the damage by dissociative electron attachment processes [18]. As the secondary electron yield is expected to be much higher for ion collisions with metal clusters than with biological molecules, the increased radiosensitive efficiency can be explained.

Also strong fragmentation and surface sputtering of metallic particles will lead to an increased metal concentration which can support the formation of radicals or increase possible toxicity effects. In general, it was shown that the sputter yield is enhanced in the case of nanoparticles compared to bulk material [6,7,19,20]. This is due to forward emission of sputtered particles and the curvature of the nanoparticle surface [21,22].

In this work we will present mass-spectrometric studies of collisions of ions in different charge states ( $q = 2$  to 25) and with different masses (from O to Xe), with free Ag nanoparticles with diameters between 3 and 10 nm in the gas phase. Whereas earlier experiments concerned studies of ion collisions with nanoparticles deposited on surfaces, the number of studies with free NPs is very limited. On the theoretical side, several works based on molecular dynamics simulations describe the sputtering of large free metallic nanoparticles by heavy-particle impact. Many theoretical studies concerned Au nanoparticles with a radius between 4 and 12.4 nm, bombarded by Au, Ga, and Xe ions in the energy range between 16 and 200 keV [6,19,20,23–26]. The sputter yields, the phenomena of collision cascades, and the collision spike sputtering are analyzed, and corresponding results are predicted by MD calculations.

## II. METHODS

Experiments were performed at accélérateur pour la physique avec des ions de basse énergie (ARIBE), the low-energy ion beam facility of grand accélérateur national d'ions

<sup>\*</sup>patrick.rousseau@unicaen.fr

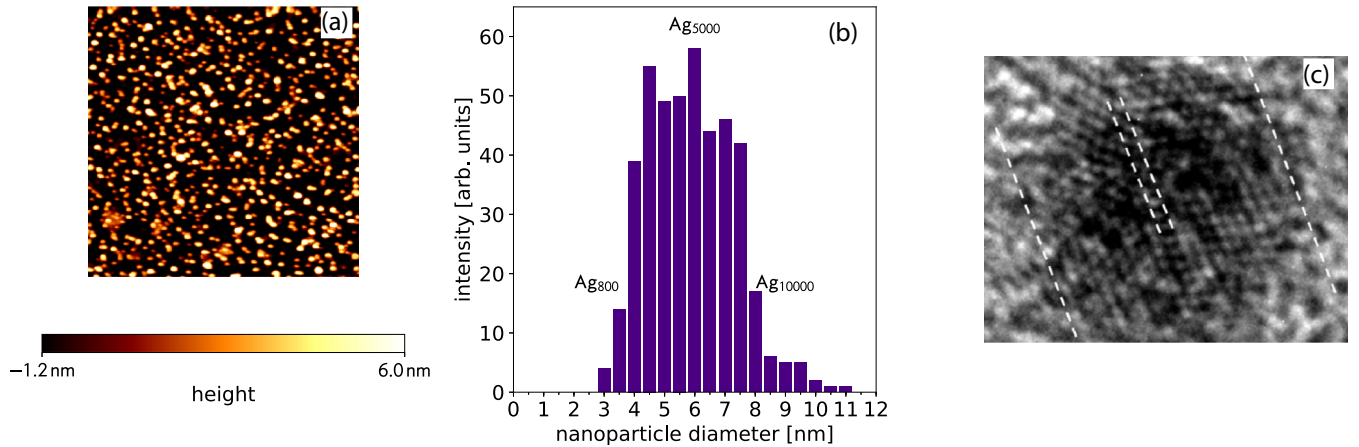


FIG. 1. (a) AFM image of Ag nanoparticles deposited on a  $\text{SiO}_2$  substrate. (b) Size histogram with a center at a diameter of about 6 nm. (c) Structure of a 5-nm Ag NP obtained by TEM microscopy.

lours (GANIL) (Caen, France). The experimental setup was described in earlier publications [27]. It is based on a crossed-beams device where a beam of multiply charged atomic ions interacts at  $90^\circ$  with a nanoparticle beam. In order to produce large metallic nanoparticles from materials with high melting points, the previous setup was modified with respect to the nanoparticle source. The former gas aggregation cluster source was replaced by a magnetron discharge sputter source which allows for the formation of beams of neutral metallic nanometer-sized particles [28]. After the collision, positively charged reaction products are extracted and analyzed with respect to their ratio of mass over charge. As nanoparticles with very high masses ( $\approx 50$  kD) are to be detected, they are postaccelerated after the time-of-flight (TOF) analysis to a plate held at a potential of  $\approx -20$  kV, and secondary electrons are guided towards a  $-18$ -kV-biased channel plate device by a weak magnetic field. The collision products are analyzed and registered on an event-by-event basis.

In order to measure the size distribution of the neutral nanoparticles, they were deposited at very low energies (several meV/atom) on a  $\text{SiO}_2$  substrate or transmission electron microscope (TEM) grids. Their size is analyzed either with an atomic force microscope (AFM) [see Fig. 1(a)], yielding the size histogram [Fig. 1(b)], or with a TEM, which revealed the particle structure, as shown in Fig. 1(c). The nanoparticle diameters extend from 3 to 10 nm, with an average size of 6 nm. This corresponds to a particle range containing between 800 and 10 000 atoms with a center at about 6600 Ag atoms. The maximum of the size distribution depends on the aggregation length in the cluster source, the gas pressure, and the current of the magnetron discharge. The TEM image shows the internal structure with atomic rows of a Ag crystal with an estimated interatomic spacing of 0.25 nm, which is expected to be  $\approx 0.21$  nm. One can observe a different line orientation within the cluster which might indicate that the cluster is formed by already preformed smaller clusters in cluster-cluster collisions. The kinetic energy of charged nanoparticles with a size of 2400 atoms has been determined to be 3.9 eV, corresponding to a velocity of  $\approx 50$  m/s. This is close to the velocity of the Ar buffer gas and should therefore also be similar for neutral particles of the same size. This has to

be taken into account when extracting the ions perpendicular to the TOF spectrometer. The detection efficiency for ions has been estimated to be 45%, which decreases towards larger particle masses, in particular when detected as singly charged ions. The density of the nanoparticle beam was estimated to be  $10^6$  to  $10^7$  particles per cubic centimeter. When we compare these values with the sputter yield in the magnetron nanoparticle source, the comparison yields an overall efficiency of the neutral beam production of  $10^{-3}$  to  $10^{-4}$ .

### III. RESULTS AND DISCUSSION

#### A. Mass spectra, multielectron capture, and cluster stability

When collision experiments with highly charged ions are performed with geometrically large targets, it is of special advantage to classify the type of collision according to the impact parameter [see Fig. 2(a)]. Thus, if the impact parameter  $b$  is larger than the nanoparticle radius  $R_{\text{NP}}$ , we call the collision “peripheral,” and the projectile interacts mainly with the electronic target system. In the present situation of low collision energies, it is the (multiple) electron capture process which dominates the interaction. For the case that the impact parameter is smaller than the nanoparticle radius, the projectile penetrates the target and interacts with both electrons and heavy nuclei. The importance of both mechanisms depends on the velocity and the mass of the projectile.

Figure 2(b) shows the geometrical cross section for penetrating collisions for Ag nanoparticles with diameters of 2 and 6 nm. The values are rather large and correspond to about  $3 \times 10^{-14}$  and  $2.7 \times 10^{-13}$   $\text{cm}^2$ . The total cross sections for peripheral electron capture, i.e., where the projectile does not penetrate the nanoparticle, were calculated within the classical over-the-barrier model (COBM) which was adapted for ion collisions with a conducting sphere [29,30], using ionization potentials containing the work function and a Coulomb term [31,32]. We obtained values between  $1 \times 10^{-13}$  and  $3 \times 10^{-13}$  and  $1.4 \times 10^{-13}$  and  $4.8 \times 10^{-13}$   $\text{cm}^2$  respectively, for particle diameters of 2 and 6 nm and for projectile charge states between 2 and 17. From the electron capture cross sections the central part  $\pi R_{\text{NP}}^2$  representing penetrating collisions was subtracted.

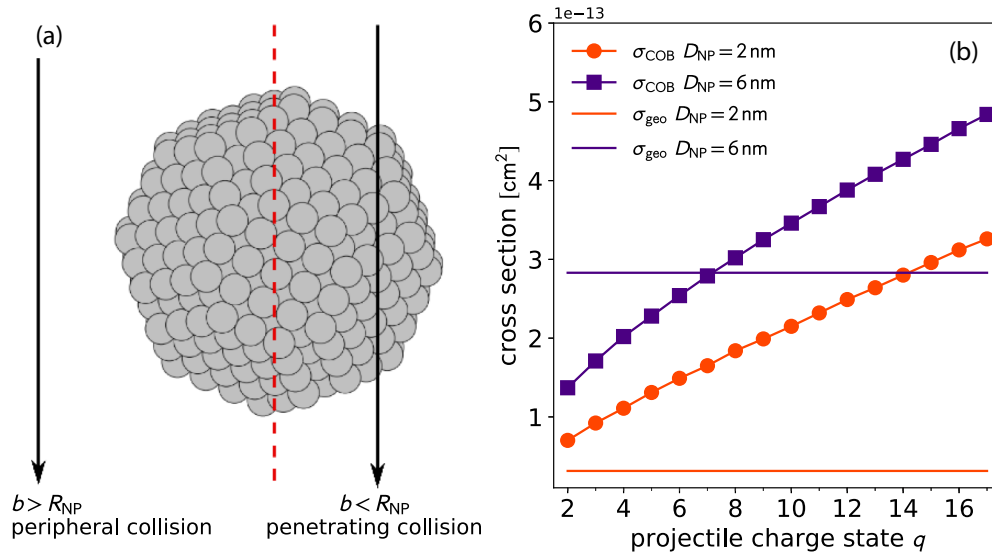


FIG. 2. (a) Scheme of the collision system, showing the impact parameter  $b$  and the nanoparticle radius  $R_{NP}$ . (b) Geometrical cross section (horizontal lines) and cross sections for the total electron capture in peripheral collisions as a function of the projectile charge, shown for two Ag nanoparticle with diameters of 2 and 6 nm.

For the smaller nanoparticle diameter, electron capture dominates in the whole range of  $q$  values, and the system behaves in a way which one would expect for ion-atom collisions. However, for 6-nm particles and low-charge-state projectiles ( $q < 8$ ) cross sections for penetrating collisions overcome those for peripheral ones, and therefore, one might expect features similar to those observed in ion-solid collisions.

In Fig. 3 the time-of-flight spectrum obtained in collisions of  $\text{Ar}^{9+}$  projectiles at 135 keV with 6-nm Ag nanoparticles is shown for flight time values of up to 400  $\mu\text{s}$ , which corresponds to clusters containing about 1100 Ag atoms. The spectrum consists of two parts: (i) an intense distribution of small fragments containing one to nine silver atoms with decreasing intensities reaching the cluster size of 21 and (ii) a broad distribution in the  $n/q$  range from 50 to 1100, which

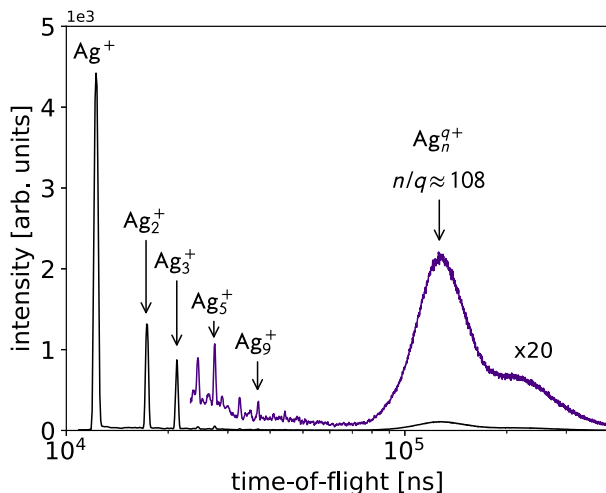


FIG. 3. Time-of-flight spectrum of silver nanoparticles produced in  $\text{Ar}^{9+}$ -Ag $_n$  collisions at a collision energy of 135 keV.

is not mass resolved and which shows a maximum at around 100 Ag atoms. Whereas the small fragments represent 25% of the total spectrum, the larger systems make up 75% due to their larger mass range. When interpreting the intensity, we have to take into account that the detection efficiency strongly decreases with increasing cluster mass; hence, the contribution from larger systems is expected to be much higher. For these reasons the distribution of the large cluster products will not be discussed further in this work.

As shown in Fig. 2, the total peripheral electron capture cross sections are large, reaching for collisions of  $\text{Ar}^{9+}$  projectiles with 6-nm Ag nanoparticles a value of  $3.3 \times 10^{-13} \text{ cm}^2$ . Therefore, we expect that electron capture occurs with high probability and produces a large number of multiply charged Ag clusters. The question arises whether these are stable before their detection or whether they decay by different processes. In order to answer this question we show in Fig. 4(a) the stability diagram for multiply charged  $\text{Ag}_n^{q+}$  systems, which represents the charge as a function of the cluster size in a double-logarithmic display. The line marked with  $n_{cr}$  separates the diagram into two regions. In the upper part, the charged systems are spontaneously unstable as no energetic barrier exists which could stabilize the system against infinitesimally small deformations leading to charge separation. In the lower part, multiply charged nanoparticles are stable if the temperature of the system is 0 K, as a finite fission barrier exists. However, for finite temperatures the system may overcome this barrier and decay in this region. The most favorable decay channel depends on the height of the fission barrier  $B_f$  compared to the activation energies  $E_a$  for other processes, for example, for the evaporation of a neutral particle. In the case that  $B_f = E_a$ , both processes occur in competition with each other, and we obtain the dot-dashed line labeled  $n_{app}$  (see Fig. 4). For large clusters the appearance size approaches the critical size as shown in fission experiments with highly charged sodium clusters [8] [see black dotted line in Fig. 4(a)].

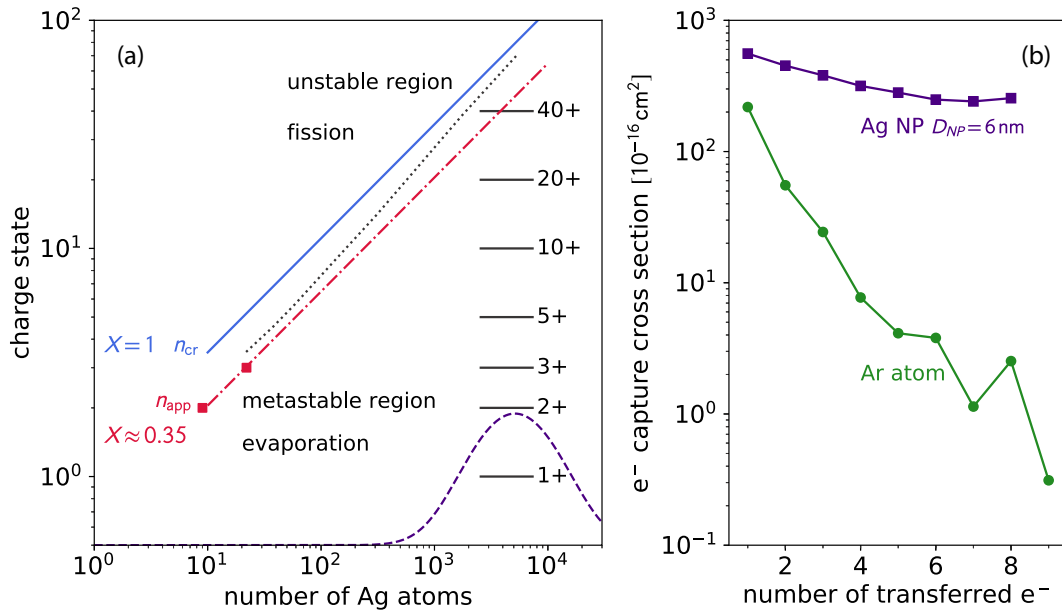


FIG. 4. (a) Stability diagram for multiply charged Ag nanoparticles. The appearance sizes for  $q = 2$  and  $q = 3$  are taken from Schulze *et al.* [33]. The size distribution of the initial nanoparticles is shown as a dashed line. (b) COB cross sections for multielectron capture by  $\text{Ar}^{9+}$  projectiles from  $\text{Ag}_n$  ( $D_{\text{NP}} = 6$  nm) and Ar atoms.

In order to discuss the ionization probability we show in Fig. 4(b) multielectron capture cross sections. The data were calculated for peripheral collisions of  $\text{Ar}^{9+}$  projectiles with 6-nm Ag nanoparticles and compared with an atomic Ar target, both calculated within the COBM [30]. For the atomic target, capture is strongly dominated by single-electron capture; the cross section decreases by a factor of about 1000 for capturing nine electrons. This is due to the strong increase of the ionization potential with the charge state of the target ( $\approx 15$  eV to 422 eV). In the case of large metallic nanoparticles (6 nm) the ionization potential increases much slower with the charge state, thus increasing from 4.6 eV for the neutral system to about 18 eV for a nanoparticle with a charge of 25. As a consequence, the multielectron capture cross section decreases only slowly with the number of transferred electrons, for example, by only a factor of 2 for the single-electron capture compared to the capture of eight electrons. A large fraction of the collisions leads to the neutralization of the projectile as observed in ion-surface collisions. From these considerations we may conclude that a high degree of ionization is obtained in peripheral collisions.

Other mechanisms may contribute to additional electron emission. As by multielectron capture multiply excited states are populated, these may rapidly decay by fast Auger processes during the collision. Thus, in earlier experiments with highly charged ions ( $\text{Xe}^{q+}$ ) colliding with  $\text{C}_{60}$  molecules, it was shown that processes with very high electron multiplicities (up to 80 electrons [34]) may occur in glancing collisions, although the production of these high charge states occurs only with rather small cross sections. Further mechanisms for electron emission may be based on thermionic electron emission [35] or the decay of multiple plasmons, depending on the degree of excitation occurring in the ion collision [17,36]. On the other hand, it was shown that for large systems

and hence characteristic large impact parameters the static COBM overestimates the final charge state due to dynamical effects [37]. It takes time for the electrons to move from the nanoparticle to the bypassing projectile. When including this effect in a so-called dynamical COBM for the system  $\text{Xe}^{25+}/\text{Na}_{196}$  collisions, good agreement is obtained with results from calculations with the Vlasov equation [37].

In Fig. 4(a) we add the initial size distribution of the neutral Ag nanoparticles (taken from Fig. 1), shown as a dashed curve. When multiply ionized by  $\text{Ar}^{9+}$  ions, these particles will be stable up to very high charge states ( $q \approx 30$ ) and can reach the unstable region only via long evaporation chains. As an example we may regard the system  $\text{Ag}_{6000}^{10+}$ , which, when hot, will start emitting neutral particles. However, in order to reach the corresponding appearance size, which is about  $n \approx 200$  for  $q = 10$ , nearly the whole particle has to be evaporated, and  $\approx 5800$  atoms have to be emitted. Taking into account the adhesion energy per atom of  $\approx 2.9$  eV, this requires a total energy of  $\approx 17$  keV, which is very unlikely to be transferred in peripheral electron capture collisions with  $\text{Ar}^{9+}$  ions. Thus, we expect that even for highly charged nanoparticles fission processes occur only with very low probability.

Concerning penetrating collisions, also here, multiply charged nanoparticles are produced by electron capture during the approaching phase. But in contrast to peripheral collisions, a large amount of energy is deposited in the nanoparticle itself. In order to roughly estimate the energy deposit we have considered the projectile energy loss calculated with the aid of the SRIM program [38] for Ag bulk material. In the case of an Ar projectile passing at 135 keV through a 6-nm Ag nanoparticle in a central collision ( $b = 0$ ), an average energy of 5 keV is deposited by nuclear stopping processes, and 4 keV is deposited by the interaction with the electronic target system. These penetrating collisions may lead to

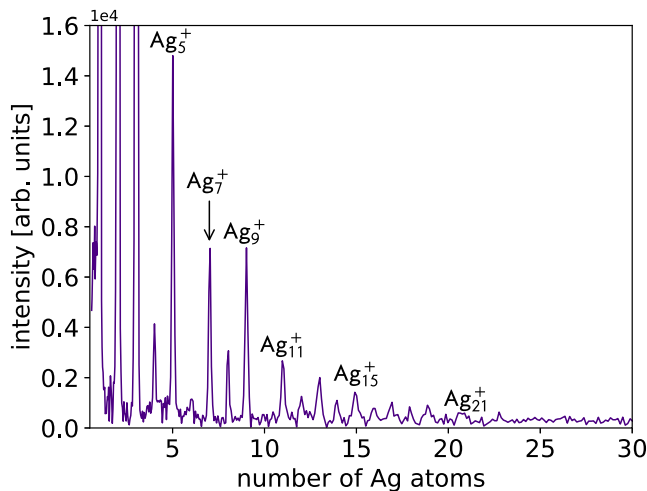


FIG. 5. Distribution of small singly charged fragments produced in collisions of  $\text{Xe}^{17+}$  projectiles with neutral Ag nanoparticles at 255 keV.

fragmentation, evaporation, and sputtering, in contrast to peripheral collisions, which form dominantly multiply charged stable Ag clusters due to the much lower energy transfer. Corresponding results were shown for collisions of ions with sodium clusters which transfer energies from 10 to several 100 eV depending on the projectile charge state and velocity [39]. The importance of penetrating collisions is particularly supported by the fact that the distribution of the product ions does not change strongly when projectiles in very low charge states are used, for example,  $\text{O}^{3+}$  ions, which will not produce very high charge states by peripheral electron capture.

### B. Small-fragment production from large Ag nanoparticles

In order to further quantify the production of small-size fragments in the case of large Ag clusters, we analyze in the following their distribution in more detail and compare the results with those obtained in ion-surface collisions. In Fig. 5 we show the distribution of small singly charged fragments produced in collisions of  $\text{Xe}^{17+}$  projectiles at 255 keV with large neutral Ag nanoparticles. Earlier measurements with clusters of fullerenes suggested that the detection efficiency does not decrease for singly charged particles with sizes up to about 3600 amu, corresponding to  $\text{Ag}_{30}^+$  clusters. This is due to the strong postacceleration towards the conversion plate in the TOF system. Therefore, no correction was necessary. We observe the dominance of singly charged monomers, dimers, and trimers (see also Fig. 3). With increasing cluster size the peak intensity decreases, in particular after the closed-shell systems with 2, 8, and 20 electrons, i.e., for singly charged ions characterized by  $n = 3, 9,$  and  $21$ . Corresponding mass spectra resulting from the sputtering of a pure silver surface by a  $\text{Xe}^+$  projectile ion at energies of 10 keV [40] and 20 keV [41] show a high degree of similarity with the present spectrum concerning the structure and shell-closing phenomena. Similar mass spectra are also observed after postionization of the neutral species emitted by sputtering of a Ag surface by 15-keV  $\text{Xe}^+$  ions [42]. In the same study, the ionic fraction of the sputtered clusters was determined as a function of their

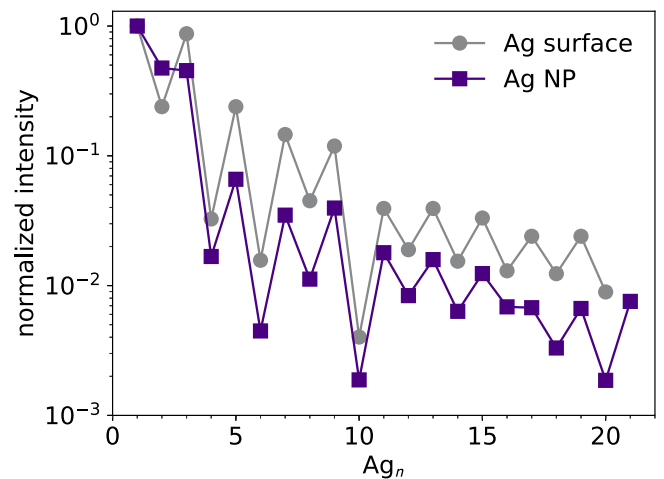


FIG. 6. Integrated peak intensities as a function of the cluster size  $n$  normalized to the monomer intensity. Squares: spectrum taken from Fig. 5(a) for  $\text{Xe}^{17+}$  ion collisions with Ag nanoparticles; dots: spectrum taken obtained in  $\text{Xe}^+$ -surface collisions [40].

size. It was shown that this fraction corresponds to about  $10^{-4}$  for monomers and dimers, and it increases with increasing cluster size. However, the ionic fraction never exceeds 10%. Nevertheless, the distribution of small size fragments also shows a maximum at the monomer and dimer.

In Fig. 6 we compare the integrated peak intensities of small fragments for free Ag nanoparticles bombarded by  $\text{Xe}^{17+}$  ions at 255 keV with those for a Ag surface irradiated by  $\text{Xe}^+$  projectiles at a collision energy of 10 keV [40]. In both cases the monomer ion is found to be the dominant fragment, as already reported for ion- or atom-surface collisions [40–42]. In general we find a very strong similarity. For both data sets, strong even-odd oscillations show up, favoring systems which are characterized by an even number of electrons, i.e., odd numbers of atoms for singly positively charged clusters. Electron pairing leads to slightly higher binding energies as well as ionization potentials and causes this phenomenon. In particular, clusters containing 6, 10, and 20 atoms are low intensity in both cases, probably due to a lower stability of the systems. All these findings indicate that large silver nanoparticles essentially behave like nanosurfaces and that sputtering phenomena are the main reason for the presence of small fragments.

Another test for this hypothesis is made by a comparison of the produced ion yields (integrated over the small systems, including the monomer, dimer, and trimer ions) with an experimental sputter yield formula established for projectiles in different charge states and kinetic energies with surfaces [43]. In Fig. 7 we show the relative fragment yields obtained with the projectiles  $\text{O}^{2+}$  (30 keV),  $\text{O}^{3+}$  (45 keV),  $\text{Ar}^{6+}$  (90 keV),  $\text{Ar}^{9+}$  (135 keV), and  $\text{Xe}^{25+}$  (255 keV). These values are normalized with respect to the Xe data of the empirical formula, and they are displayed as a function of the product of the square root of the mass  $m$  and the inverse projectile velocity  $v$ . In the present parameter range this product is close to the nuclear stopping power, which is the main mechanism for sputtering events. The good agreement between both data sets underlines that surface sputtering is the main mechanism for producing small

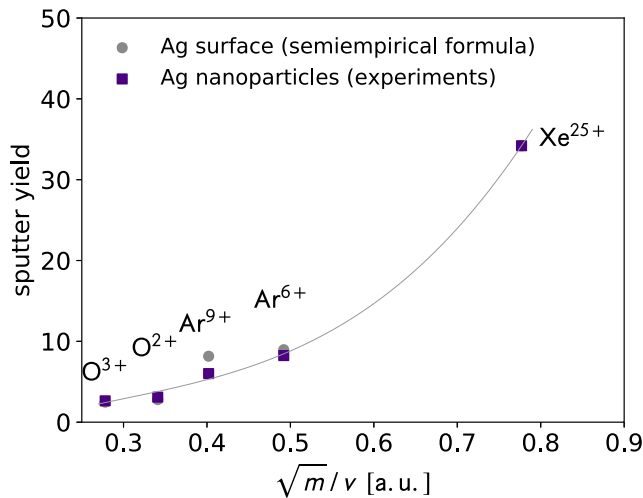


FIG. 7. Comparison of sputter yields. The values are normalized to that for collisions with  $\text{Xe}^{25+}$  projectiles. Squares: integrated intensities for monomers, dimers, and trimers measured in the present experiment for different projectiles; dots: yield values calculated with the empirical formula for ion/Ag-surface collisions [43].

fragments when large metallic nanoparticles are bombarded with ions.

It should be mentioned that for other collision systems sputtering phenomena have been studied theoretically. Accordingly, the sputter yield for nanoparticles may be larger than that for a surface. This was shown for Ga atoms colliding with Au nanoparticles where a maximum of the sputter yield is predicted for a particle diameter of 6 nm, for which it may overcome the yield for a gold surface by a factor of about 4 [25].

#### IV. CONCLUSION

The interaction of multiply charged ions with large metallic NPs, studied in the gas phase, is characterized by several mechanisms. Their relative role depends on the NP diameter and the charge of the impinging projectile. In the case of a 6-nm Ag NP the geometrical cross is of the order of  $2.8 \times 10^{-13} \text{ cm}^2$ , provoking penetrating collisions. This value is larger than the electron capture cross section for peripheral collisions of multiply charged  $\text{A}^{q+}$  ions if the charge state is below  $q = 8$ . On the other hand, as the electron capture

cross section does not decrease strongly with the number of captured electrons, multielectron capture processes are expected to be essential and to produce also highly charged nanoparticles.

The measured mass-over-charge distribution of the produced ions contains two parts: large clusters or residues are expected to be highly charged; however, they are, in most cases, stable on the experimental timescale due to the large cluster size. These can be formed in peripheral collisions, but also contributions from penetrating collisions are present as similar spectra are observed for low projectile charge states ( $\text{O}^{3+}$ ).

The small-size fragment distribution is dominated for all projectile charge states by the monomer ion. This is different from systems where fission processes are dominant. Thus, for smaller clusters ( $\text{Bi}_{(80)}$ ) the emission of the trimer becomes dominant for low-charge-state projectiles [28]. Furthermore, the distribution resembles strongly that obtained in corresponding ion/Ag-surface collisions; also the measured yield of small fragments agrees well with an empirical formula established for sputter yields from ion-irradiated Ag surfaces. Therefore, we conclude that a 6-nm nanoparticle behaves in the present collision event like a nanosurface where sputtering becomes more important than electron capture concerning the production of small fragments.

Concerning radiosensitizing effects, we believe that in addition to the increased emission of secondary electrons, also the increased density of Ag particles (fragments in the form of Ag atoms and small Ag clusters) may play an important role, for example, by provoking toxicity effects.

#### ACKNOWLEDGMENTS

The research was conducted in the framework of the International Associated Laboratory (LIA) “Fragmentation DYNAMics of complex MOlecular systems – DYNAMO,” funded by the Centre National de la Recherche Scientifique and in the frame of the COST action CM1204 “XUV/X-ray light and fast ions for ultrafast chemistry (XLIC).” A.P.M. was funded by the European Union Seventh Framework Programme under Grant Agreement No. 608163 (PEOPLE2013-ITN-ARGENT project: Advanced radiotherapy generated by exploiting nanotechnology). We further acknowledge the technical support by J.-M. Ramillon, C. Feierstein, T. Been, and the aid of I. Monnet during the AFM and TEM measurements.

[1] A. V. Krasheninnikov and K. Nordlund, *J. Appl. Phys.* **107**, 071301 (2010).  
 [2] U. Kirchner, R. Vogt, C. Natzeck, and J. Goschnick, *J. Aerosol Sci.* **34**, 1323 (2003).  
 [3] E. M. Bringa, S. O. Kucheyev, M. J. Loeffler, R. A. Baragiola, A. G. G. M. Tielens, Z. R. Dai, G. Graham, S. Bajt, J. P. Bradley, C. A. Dukes *et al.*, *Astrophys. J.* **662**, 372 (2007).  
 [4] T. T. Järvi, D. Pohl, K. Albe, B. Rellinghaus, L. Schultz, J. Fassbender, A. Kuronen, and K. Nordlund, *Europhys. Lett.* **85**, 26001 (2009).

[5] A. Klimmer, P. Ziemann, J. Biskupek, U. Kaiser, and M. Flesch, *Phys. Rev. B* **79**, 155427 (2009).  
 [6] L. Yang, M. P. Seah, E. H. Anstis, I. S. Gilmore, and J. L. S. Lee, *J. Phys. Chem. C* **116**, 9311 (2012).  
 [7] G. Greaves, J. A. Hinks, P. Busby, N. J. Mellors, A. Ilinov, A. Kuronen, K. Nordlund, and S. E. Donnelly, *Phys. Rev. Lett.* **111**, 065504 (2013).  
 [8] F. Chandezon, C. Guet, B. A. Huber, D. Jalabert, M. Maurel, E. Monnard, C. Ristori, and J. C. Rocco, *Phys. Rev. Lett.* **74**, 3784 (1995).

- [9] F. Chandezon, C. Guet, B. A. Huber, D. Jalabert, M. Maurel, E. Monnard, C. Ristori, and J. C. Rocco, *Surf. Rev. Lett.* **3**, 529 (1996).
- [10] C. Bréchnignac, P. Cahuzac, F. Carlier, and M. de Frutos, *Phys. Rev. Lett.* **64**, 2893 (1990).
- [11] C. Bréchnignac, P. Cahuzac, F. Carlier, M. de Frutos, R. N. Barnett, and U. Landman, *Phys. Rev. Lett.* **72**, 1636 (1994).
- [12] C. Bartels, C. Hock, J. Huwer, R. Kuhnen, J. Schwöbel, and B. von Issendorff, *Science* **323**, 1323 (2009).
- [13] M. Bolsa Ferruz, V. Ivošev, K. Haume, L. Ellis-Gibblings, A. Traore, V. Thakare, S. Rosa, P. de Vera, V.-L. Tran, A. Mika *et al.*, *New Research in Ionizing Radiation and Nanoparticles: The ARGENT Project* (Springer, Cham, 2017), pp. 379–434.
- [14] S. Lacombe, E. Porcel, and E. Scifoni, *Cancer Nanotechnol.* **8**, 9 (2017).
- [15] E. Porcel, S. Liehn, H. Remita, N. Usami, K. Kobayashi, Y. Furusawa, C. Le Sech, and S. Lacombe, *Nanotechnology* **21**, 085103 (2010).
- [16] Y. Liu, P. Zhang, F. Li, X. Jin, J. Li, W. Chen, and Q. Li, *Theranostics* **8**, 1824 (2018).
- [17] A. V. Verkhovtsev, A. V. Korol, and A. V. Solov'yov, *J. Phys. Chem. C* **119**, 11000 (2015).
- [18] B. Boudaiffa, P. Cloutier, D. Hunting, M. A. Huels, and L. Sanche, *Science* **287**, 1658 (2000).
- [19] R. Kissel and H. M. Urbassek, *Int. J. Mass Spectrom.* **208**, 29 (2001).
- [20] T. T. Järvi, J. A. Pakarinen, A. Kuronen, and K. Nordlund, *Europhys. Lett.* **82**, 26002 (2008).
- [21] M. L. Nietiadi, L. Sandoval, H. M. Urbassek, and W. Möller, *Phys. Rev. B* **90**, 045417 (2014).
- [22] H. M. Urbassek, R. M. Bradley, M. L. Nietiadi, and W. Möller, *Phys. Rev. B* **91**, 165418 (2015).
- [23] S. Zimmermann and H. M. Urbassek, *Int. J. Mass Spectrom.* **272**, 91 (2008).
- [24] T. Järvi and K. Nordlund, *Nucl. Instrum. Methods Phys. Res., Sect. B* **272**, 66 (2012).
- [25] L. Sandoval and H. M. Urbassek, *Nanoscale Res. Lett.* **10**, 314 (2015).
- [26] M. Li, Q. Hou, J. Cui, and J. Wang, *Nucl. Instrum. Methods Phys. Res., Sect. B* **425**, 43 (2018).
- [27] T. Bergen, X. Biquard, A. Brenac, F. Chandezon, B. A. Huber, D. Jalabert, H. Lebius, M. Maurel, E. Monnard, J. Opitz *et al.*, *Rev. Sci. Instrum.* **70**, 3244 (1999).
- [28] A. Mika, P. Rousseau, A. Domaracka, and B. A. Huber, *Phys. Rev. A* **99**, 012707 (2019).
- [29] H. Cederquist, A. Fardi, K. Haghghat, A. Langereis, H. T. Schmidt, S. H. Schwartz, J. C. Levin, I. A. Sellin, H. Lebius, B. Huber *et al.*, *Phys. Rev. A* **61**, 022712 (2000).
- [30] H. Zettergren, H. T. Schmidt, H. Cederquist, J. Jensen, S. Tomita, P. Hvelplund, H. Lebius, and B. A. Huber, *Phys. Rev. A* **66**, 032710 (2002).
- [31] C. Bréchnignac, P. Cahuzac, F. Carlier, J. Leygnier, and A. Sarfati, *Phys. Rev. B* **44**, 11386 (1991).
- [32] U. Näher, S. Bjørnholm, S. Frauendorf, F. Garcias, and C. Guet, *Phys. Rep.* **285**, 245 (1997).
- [33] W. Schulze, B. Winter, and I. Goldenfeld, *Phys. Rev. B* **38**, 12937 (1988).
- [34] S. Martin, R. Brédy, J. Bernard, J. Désesquelles, and L. Chen, *Phys. Rev. Lett.* **89**, 183401 (2002).
- [35] J. U. Andersen, E. Bonderup, and K. Hansen, *J. Phys. B: At. Mol. Opt. Phys.* **35**, R1 (2002).
- [36] L. G. Gerchikov, C. Guet, and A. N. Ipatov, *Phys. Rev. A* **66**, 053202 (2002).
- [37] L. Plagne and C. Guet, *Phys. Rev. A* **59**, 4461 (1999).
- [38] J. F. Ziegler, M. Ziegler, and J. Biersack, *Nucl. Instrum. Methods Phys. Res., Sect. B* **268**, 1818 (2010).
- [39] J. Daligault, F. Chandezon, C. Guet, B. A. Huber, and S. Tomita, *Phys. Rev. A* **66**, 033205 (2002).
- [40] I. Katakuse, T. Ichihara, Y. Fujita, T. Matsuo, T. Sakurai, and H. Matsuda, *Int. J. Mass Spectrom. Ion Processes* **67**, 229 (1985).
- [41] W. Harbich and C. Félix, *C. R. Phys.* **3**, 289 (2002).
- [42] C. Staudt, R. Heinrich, and A. Wucher, *Nucl. Instrum. Methods Phys. Res., Sect. B* **164–165**, 677 (2000).
- [43] N. Matsunami, Y. Yamamura, Y. Itikawa, N. Itoh, Y. Kazumata, S. Miyagawa, K. Morita, R. Shimizu, and H. Tawara, *At. Data Nucl. Data Tables* **31**, 1 (1984).